Thermal Annealing of Fluorocarbon Films Grown by Hot Filament Chemical Vapor Deposition

Kenneth K. S. Lau and Karen K. Gleason*

Department of Chemical Engineering, Massachusetts Institute of Technology, Cambridge, Massachusetts 02139

Received: June 30, 2000; In Final Form: December 6, 2000

Annealing alters the stability, structure, and morphology of fluorocarbon films grown from hot filament chemical vapor deposition (HFCVD) using hexafluoropropylene oxide (HFPO) precursor. The composition of these films is greater than 97% CF_2. The as-deposited film in this study contains extraneous hydroxyl (OH) and carbonyl/carboxyl (CO/COO) groups, as revealed by Fourier transform infrared (FTIR) spectroscopy. Such groups are found to be thermally labile and lead to two film decomposition regimes, centered at 150 and 300 °C. This is similar to the two decomposition onsets at 150−250 and 300 °C observed in irradiated bulk PTFE, which are attributed to the loss of peroxy radicals and COOH groups, respectively. A postdeposition 1 h 400 °C in situ vacuum anneal reduced the OH and CO/COO groups in the HFCVD film to below FTIR detection limits. This postanneal film is found to be stable up to 400 °C with no evidence of structural changes. The surface morphology of the film quenched from the 1 h 400 °C in situ vacuum anneal, as imaged by optical microscopy (OM), resembles that of the as-deposited film, showing no discernible surface features. However, for a film quenched from the 1 h 325 °C in situ vacuum anneal, significant crystalline spherulites of up to ∼1 mm in diameter are observed through OM. This is attributed to favorable crystallization in the proximity of the melting temperature of bulk PTFE. Intensity differences in FTIR absorption peaks in this film, compared to the other films, also support the morphological differences seen.

I. Introduction

Poly(tetrafluoroethylene) (PTFE, $(CF_2)_n$), unlike other common homopolymers, exhibits unique properties that requires the use of special methods for processing into thin films. Its insolubility in most solvents precludes film deposition by casting or spin-coating methods.[1] W. L. Gore & Associates recently demonstrated spin coating of PTFE thin films, albeit using aqueous nanoemulsions of solid PTFE particles followed by high-temperature sintering.[2] Most of the effort to deposit PTFE thin films therefore concentrates on gas-phase techniques.

Pulsed laser deposition (PLD) can yield high-quality PTFE thin films.[3−5] UV irradiation of PTFE targets is believed to cause depolymerization and chain unzipping into the monomer through local heating with subsequent repolymerization of the monomer on a substrate surface.[3] It is suggested that this thermally driven process applies to polished PTFE pellet targets, while for pressed powder targets, deposition is believed to be a transfer of PTFE grains followed by melting and recrystallization on a heated substrate.[5] Other radiation sources, such as synchrotron ablation, give similar PTFE films, although perhaps of lower molecular weight since CF_3 is observed.[6,7]

As direct pyrolysis of PTFE is known to cause chain unzipping into the monomer, PTFE films can be formed by redeposition downstream of the pyrolysis zone.[8,9] Spectroscopic characterization shows these films to be consistent with the bulk material.[9] In an extension to this technique, PTFE films are also formed by ionizing some of the evaporated material and electrically accelerating them toward a biased substrate surface.[10] Other attempts in making PTFE films include plasma polymerization of fluorocarbon gases and plasma sputtering of PTFE targets.[11] However, in most of these cases, resulting films are not "clean", containing a variety of CF_x bonding environments, which indicates a highly cross-linked network. The exception is downstream fluorocarbon plasma deposition in which films approaching PTFE can be produced, although even in such cases films still contain a significant fraction (>10%) of CF_3.[12,13]

Recently, hot filament chemical vapor deposition (HFCVD) has been demonstrated as a method to produce films with >97% linear CF_2 chains.[14−16] Hexafluoropropylene oxide (HFPO, CF_3-$CF(O)CF_2$) is used as the precursor gas since it is known to thermally decompose into difluorocarbene (CF_2) diradicals and a stable trifluoroacetyl fluoride gas (CF_3CFO) (eq 1), with subsequent polymerization of the CF_2 diradicals to form linear PTFE chains (eq 2).[17−19] HFCVD has the advantage of independent control over the temperature of the heated filament wires to initiate gas decomposition and the temperature of the substrate where film deposition occurs. The latter can be kept low to facilitate adsorption of polymerizing species and enhance film growth. Studies have been made to investigate the structure−property−processing relationships of HFPO HFCVD films.[20,21]

$$CF_3CF(O)CF_2 \xrightarrow{\triangle} CF_2 + CF_3CFO \quad (1)$$

$$nCF_2 \rightarrow (CF_2)_n \quad (2)$$

In this paper we present the effect of postdeposition annealing on HFPO HFCVD film stability, structure, and morphology. The thermal decomposition and melting behavior in these films will be compared to those for bulk PTFE. Thermal stability is important especially when these films have the potential of being integrated into microelectronic circuits as future low dielectric

* To whom correspondence should be addressed. E-mail: kkgleasn@mit.edu.

10.1021/jp002347u CCC: $20.00
Published on Web 03/06/2001

TABLE 1: HFPO HFCVD Film Samples

sample	film thermal history
DEP	as-deposited[a]
A325	as-deposited[a] → 1 h 325 °C in situ vacuum-annealed → quenched
A400	as-deposited[a] → 1 h 400 °C in situ vacuum-annealed → quenched

[a] 1 h deposition at 1.0 Torr, 15 sccm, and 15 min filament preconditioning. Filament temperature at 500 ± 50 °C.

constant (κ) materials, since bulk PTFE has one of the lowest κ values (2.1[22]) for a nonporous material.

II. Experimental Section

HFCVD was performed on 100 mm diameter silicon wafers using undiluted HFPO ($CF_3CF(O)CF_2$; DuPont) as the precursor gas. Details of the deposition chamber and filament setup have been given elsewhere.[14−16] Pristine films were deposited at 1.0 Torr of pressure, a 15 sccm flow rate, and a 15 min filament preconditioning time. Preconditioning refers to the burning in of the filament wire at the process condition prior to film deposition. The deposition time was 1 h. The filament temperature was 500 ± 50 °C, while the substrate temperature was maintained at 21 ± 5 °C using backside water cooling. Some of the pristine films were then annealed in situ using a substrate heater within the CVD chamber, which allowed annealing without breaking the vacuum. Isothermal anneals at 325 and 400 °C were performed for 1 h in a vacuum of <10 mTorr. The annealed films were subsequently quenched to room temperature at equivalent cooling rates through radiative cooling without any break in the vacuum. Table 1 summarizes the pristine and annealed film samples studied in this work.

Film samples, subsequently exposed to the atmosphere, were assessed on their thermal stability using an interferometry for thermal stability (ITS) apparatus.[23,24] ITS monitored the raw interferometry signal of a HeNe (λ = 632.8 nm) laser beam being reflected off the film as a function of time and temperature. The temperature was ramped up to 400 °C over 30 min and then maintained at the temperature setpoint for 1 h before quenching. Nitrogen was used to purge the ITS apparatus continuously. Any film thickness loss would result in a time modulation of the raw signal. To visually capture the onset of thermal decomposition, the time derivative of the laser signal was traced with a temperature ramp to the setpoint, so any deviation of the signal derivative from zero would indicate film loss and show the temperatures at which decomposition occurred.

Fourier transform infrared (FTIR) spectra of the films were acquired on a Nicolet Magna 860 under transmission in a nitrogen-purged chamber using a DTGS KBr detector for 64 averages over the range of 400−4000 cm^{-1} at 4 cm^{-1} resolution. Optical micrographs of the films were acquired using a Kramer Scientific Leitz DMRX with a CCD camera attachment under transmission mode.

III. Results and Discussion

Film Thermal Stability. Figure 1 shows the ITS trace of the time derivative of the laser signal as a function of the temperature ramp up for sample **DEP**. Figure 1 reveals the as-deposited HFPO HFCVD film (**DEP**) having two major decomposition regimes, centered at approximately 150 and 300 °C, since around these temperatures there is a significant deviation of the time derivative of the signal from zero. In contrast, the postdeposition 1 h 400 °C in situ vacuum-annealed film (**A400**) is thermally stable up to 400 °C in the ITS test, showing no deviation of the time derivative of the signal from zero (figure omitted). To understand the reasons for the difference in film thermal stability, it is helpful to look at the structure of each film before and after the ITS experiment.

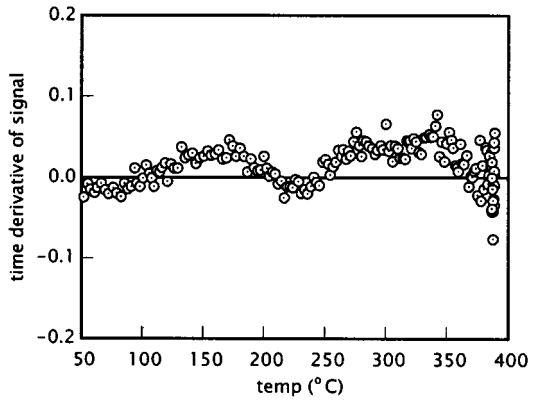

Figure 1. Time derivative of the ITS interferometry signal intensity versus temperature for the as-deposited HFPO HFCVD film (**DEP**). There are two major decomposition regimes, centered at approximately 150 and 300 °C, showing significant deviation of the signal derivative from zero.

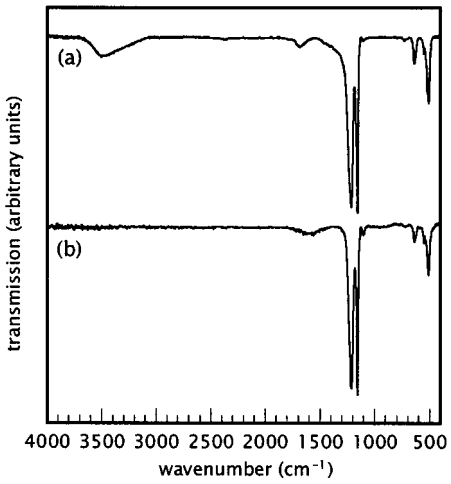

Figure 2. FTIR spectra of the thermally labile **DEP** film (a) prior to and (b) after the ITS test shown in Figure 1. The film contains thermally labile OH and CO/COO groups that are lost after the ITS test.

TABLE 2: Peak Assignments of FTIR Spectra of HFPO HFCVD Films

wavenumber (cm^{-1})	peak assignment	wavenumber (cm^{-1})	peak assignment
513/530	CF_2 rock	1215	CF_2 asymmetric stretch
555	CF_2 deformation	~1700	C═O/COO in CF_xCOO^-
641/629	CF_2 wag	~3500	OH
1155	CF_2 symmetric stretch		

Film Structural Stability. Parts a and b of Figure 2 represent the FTIR spectra of the thermally unstable **DEP** film prior to and after the ITS test. The FTIR spectra (figure omitted) of the thermally stable **A400** film prior to and after the ITS test are spectroscopically identical and resemble that of Figure 2b, the **DEP** film after the ITS test. Table 2 summarizes the FTIR peak assignments based on published literature.[25−28] All the spectra contain the CF_2 symmetric (1155 cm^{-1}) and asymmetric stretches (1215 cm^{-1}), and the lower wavenumber CF_2 rocking (513/530 cm^{-1}), deformation (555 cm^{-1}), and wagging (641/629 cm^{-1}) modes. These vibrational modes are also observed in bulk PTFE.[29] Previous solid-state nuclear magnetic resonance (NMR) studies show HFPO HFCVD films to contain >97% linear $CF_2CF_2CF_2$ structures.[15,16] These films are unlike fluo-

rocarbon plasma-deposited films with a significant CF_2 (>65%) fraction, which lack the lower wavenumber FTIR CF_2 modes, even though the CF_2 stretches are observed.[15,30] The absence of the lower wavenumber absorptions in the plasma films is attributed to network cross-links, revealed through solid-state NMR,[31,32] which may hinder such modes.[30] The present HFPO HFCVD films, which show no such cross-links and exhibit the lower wavenumber modes,[15,16] would therefore be expected to have properties more akin to bulk PTFE.

Looking first at the FTIR spectra of the films before being subjected to the ITS test, the major difference between the **DEP** and **A400** films is that the spectrum of the thermally unstable **DEP** film (Figure 2a) contains broad absorptions in the 3500 and 1700 cm^{-1} regions, corresponding to hydroxyl (OH) and carbonyl/carboxyl (CO/COO) groups, respectively, which are absent in the spectrum of the thermally stable **A400** film (figure omitted). The degree of oxygen and hydrogen incorporation in as-deposited films has been shown previously to be influenced by the conditions used for film deposition.[20] Such incorporation in the present **DEP** film (the as-deposited pristine film) can come from several possible sources.[20] The presence of background oxygen and water within the CVD chamber during deposition cannot be ruled out. Oxygen derived from the HFPO precursor may also be incorporated into the film. Postdeposition exposure to atmospheric oxygen and water can also lead to such incorporation. Regardless of the source of incorporation, the presence of OH and CO/COO groups is similar to the way in which irradiated bulk PTFE incorporates OH and CO/COO groups.

Electron spin resonance (ESR) spectroscopy of vacuum-irradiated PTFE identified relatively stable free radicals, either at chain ends as $-CF_2-CF_2^{\bullet}$ groups or along the chains as $-CF_2-CF\bullet-CF_2-$ groups.[33−37] However, these radicals react readily with oxygen upon atmospheric exposure or during irradiation in air, to form peroxy radicals, $-CF_2-CF_2OO\bullet$ and $-CF_2-CF(OO\bullet)-CF_2-$ groups, respectively.[38,39] These groups can further decompose or react with water to form −COF and −COOH groups, as evidenced by FTIR.[40,41] Such a reaction mechanism for incorporating OH and CO/COO may also be occurring in the HFPO HFCVD films. The possibility of unterminated radicals for such reactions is already hinted at by the polymerization reaction proposed in eq 2. This polymerization process would leave unterminated radicals at the ends of the $(CF_2)_n$ chains since there is no reasonable termination reaction, and would result in the formation of OH and CO/COO groups much like that discussed for irradiated bulk PTFE. This is one reasonable hypothesis to account for OH and CO/COO in the **DEP** film (Figure 2a).

The absence of OH and CO/COO FTIR peaks in the **A400** film (figure omitted) implies that the postdeposition 1 h 400 °C in situ vacuum anneal of the film prior to breaking the vacuum significantly reduced the concentration of chain end radicals, on the basis of the suggested hypothesis. This reduction to below FTIR detection limits may conceivably come through two ways. The volatilization of lower molecular weight CF_2 chains would result in a thermally stable film of higher molecular weight chains such as bulk PTFE, which has a reported weight loss of <0.01% per hour at temperatures up to 400 °C, even in 50% RH (relative humidity) air.[42] The joining of chain end radicals on two separate chains to form a longer chain would also result in more thermally stable chains for the same reason. The high-temperature anneal (400 °C) above the melting temperature of bulk PTFE (327 °C[22]) would probably provide sufficient chain mobility for such a process to occur. It is likely that both these mechanisms for reducing chain end radicals may be taking place.

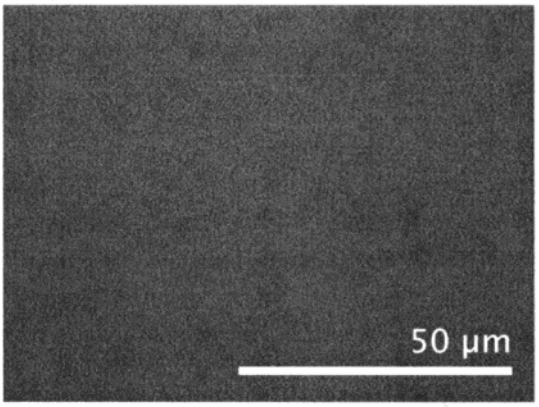

Figure 3. Optical micrograph of the as-deposited HFPO HFCVD film (**DEP**). No surface features are discernible. At 100× magnification.

Concentrating now on the FTIR spectra of the films after being subjected to the ITS test, the OH and CO/COO peaks in the spectrum of the thermally unstable **DEP** film (Figure 2b) has completely disappeared, and the whole spectrum looks similar to that of the thermally stable **A400** film (figure omitted). This implies that OH and CO/COO groups are inherently thermally labile. Indeed, thermal studies of irradiated bulk PTFE identified two major onsets of decomposition, one at around 150−250 °C and another above 300 °C.[43] These decomposition temperatures correspond remarkably well with those observed from the ITS trace of the thermally labile **DEP** film (Figure 1). The first onset is attributed to the decomposition of peroxy radicals, while the second onset is attributed to the decarboxylation of COOH groups.[43] These degradation processes may possibly occur in the **DEP** film during the ITS test since these thermally labile groups are observed to disappear after the ITS test (compare parts a and b of Figure 2).

In contrast, a lack of these groups in the thermally stable **A400** film most likely explains its thermal stability during the ITS trace (figure omitted), since no FTIR peaks disappear and no new FTIR peaks form after the ITS test (figure omitted). Discussion is withheld on the peaks at ∼1600 and 1100 cm^{-1} since no reasonable literature assignments have been found for these peaks. Further investigation is required to identify the sources of these vibrational modes. Presumably these modes are related to CF_2 bond vibrations since these modes are evident in films in which there is no evidence of OH and CO/COO groups.

Film Morphology. Optical microscopy provided a facile yet vivid means to capture the surface morphology of HFPO HFCVD films, locked in place as a result of quenching from various postdeposition in situ isothermal vacuum anneals. Figure 3 shows the as-deposited **DEP** film and at 100× magnification seems to be void of any noticeable surface characteristics. In contrast, Figure 4 reveals relatively large crystalline spherulites (∼1 mm in diameter) visible even to the naked eye for the **A325** film, quenched after a postdeposition 1 h 325 °C in situ vacuum anneal. Figure 4a, at 40× magnification, shows a spherulite grain. Parts b and c of Figure 4, at 100× magnification, show the same grain toward the edge and at the center, respectively. The optical micrograph of the surface of the **A400** film (figure omitted), quenched after a postdeposition 1 h 400 °C in situ vacuum anneal, shows no noticeable crystalline morphology and is more like the **DEP** film in Figure 3.

The growth of crystalline spherulites seems to be favored at an annealing temperature of 325 °C (Figure 4). This temperature

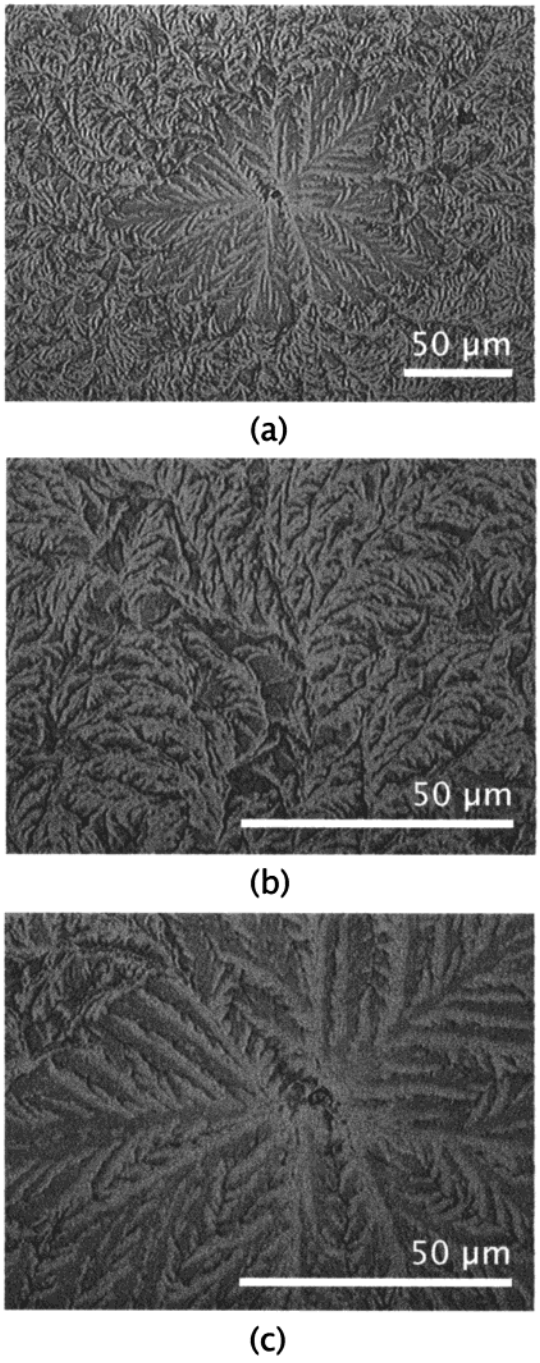

Figure 4. Optical micrographs of the HFPO HFCVD film quenched after a postdeposition 1 h 325 °C in situ vacuum anneal (**A325**). The observed crystalline spherulites, with diameters of up to ~1 mm, are attributed to crystallization near the melting point of bulk PTFE prior to quenching. At (a) 40×, (b) 100×, and (c) 100× magnifications, showing a sample grain, the grain edge, and the grain center, respectively.

is in proximity to the melting or crystallization temperature of bulk PTFE at 327 °C.[22] Significant crystallization kinetics of bulk PTFE are found to occur over a narrow supercooling temperature range of 315−325 °C.[44] It is likely that, during the postdeposition 1 h 325 °C in situ vacuum anneal, there may be similar favorable crystallization kinetics, in terms of time and temperature, for the deposited PTFE chains on the **A325** film to form these relatively large spherulites, which are locked in place upon quenching. Interestingly, comparable spherulitic growth morphologies are observed in postdeposition annealing of PLD PTFE films.[5] Further, crystalline growth at a small

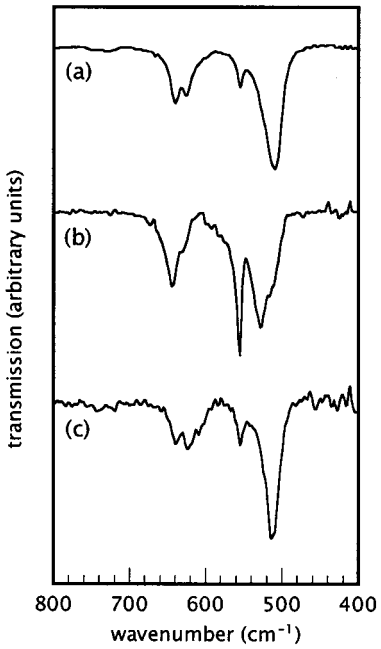

Figure 5. FTIR spectra of the (a) **DEP**, (b) **A325**, and (c) **A400** HFPO HFCVD films. The **A325** film shows significantly different absorption intensities compared to the other two films in the 400−800 cm^{-1} wavenumber region, and parallels the observed differences in crystallinity.

degree of supercooling is thought to result in fewer crystallites of larger size (as opposed to more crystallites of smaller size at a high degree of supercooling) because thermal agitation makes nucleation difficult but facilitates growth due to easier chain movement.[45] In contrast, the **A400** film, quenched from a postdeposition 1 h 400 °C in situ vacuum anneal (figure omitted), shows no noticeable crystalline spherulites. Presumably, at a temperature markedly above the crystallization temperature, the PTFE chains become too mobile to arrange into a crystalline matrix, which upon quenching are locked in their disordered melt state.[44] As such, the **A400** film resembles the as-deposited **DEP** film (Figure 3) in having no discernible crystalline morphology.

Comparison of CF_2 wagging, deformation, and rocking modes at the lower wavenumbers in the FTIR spectra (Figure 5) also provides strong evidence for changes in film crystallinity. Parts a and c of Figure 5, for the **DEP** film and the **A400** film, respectively, show similar absorption intensities. In contrast, Figure 5b, for the **A325** film, shows distinct intensity differences when compared with parts a and c of Figure 5. In particular, the doublet at 641/629 cm^{-1} shows a skew toward the former peak, while the three peaks at 555/530/513 cm^{-1} show a skew toward the former two peaks. This behavior is also observed when FTIR spectra of powder and single-crystal $C_{20}F_{42}$ are compared.[29] Thus, the apparent changes in absorption intensities can be attributed to a change from an amorphous to a highly crystalline state. This agrees well with the changes in corresponding film morphologies under optical microscopy (OM).

IV. Conclusions

The thermal stability of HFPO HFCVD films can be limited by OH and CO/COO incorporation. With a high concentration of OH and CO/COO groups, the as-deposited film in this study displays two decomposition regimes, centered at temperatures of 150 and 300 °C. Similar decomposition temperatures are observed for irradiated bulk PTFE, with the lower temperature decomposition being attributed to the loss of peroxy radicals and the higher temperature decomposition being attributed to

the loss of COOH groups. The disappearance of OH and CO/COO FTIR absorptions after the ITS test shows that these groups are also thermally labile in the as-deposited film. In contrast, with undetectable concentrations of OH and CO/COO groups after a 1 h 400 °C in situ vacuum anneal, this postanneal film is thermally stable up to 400 °C under ITS testing.

Crystallization can be induced by quenching a film from a 1 h 325 °C in situ vacuum anneal. This treatment results in the growth of spherulites having diameters of up to ~1 mm. The CF_2 rocking, deformation, and wagging FTIR modes at lower wavenumbers also reflect this structural rearrangement. The appearance of spherulites is attributed to favorable crystallization near the melting point of bulk PTFE. However, quenching a film from a 1 h 400 °C in situ vacuum anneal results in a surface morphology and lower wavenumber FTIR modes which resemble those of the as-deposited film. The lack of spherulites is attributed to a kinetically limited crystallization during quenching from this high temperature.

Acknowledgment. We gratefully acknowledge financial support from the NSF/SRC Engineering Research Center for Environmentally Benign Semiconductor Manufacturing, and the MARCO Focused Research Center on Interconnects funded at the Massachusetts Institute of Technology through a subcontract from the Georgia Institute of Technology. We thank Brett Cruden for his assistance with the ITS experiments and Xueping Jiang for her help with OM. This work also made use of the MRSEC Shared Facilities supported by the NSF (Grant DMR-9400334).

References and Notes

(1) Scheirs, J. Fluoropolymer Coatings (New Developments). In *Polymeric Materials Encyclopedia*; Salamone, J. C., Ed.; CRC Press: Boca Raton, FL, 1996; Vol. 4, p 2498.
(2) Sun, S. C.; Chiang, Y. C.; Rosenmayer, C. T.; Teguh, J.; Wu, H. *Mater. Res. Soc. Symp. Proc.* **1997**, *443*, 85.
(3) Blanchet, G. B.; Fincher, C. R.; Jackson, C. L. Jr.; Shah, S. I.; Gardner, K. H. *Science* **1993**, *262*, 719.
(4) Jiang, W.; Norton, M. G.; Tsung, L.; Dickinson, J. T. *J. Mater. Res.* **1995**, *10*, 1038.
(5) Li, S. T.; Arenholz, E.; Heitz, J.; Bauerle, D. *Appl. Surf. Sci.* **1998**, *125*, 17.
(6) Katoh, T.; Zhang, Y. *Appl. Phys. Lett.* **1996**, *68*, 865.
(7) Katoh, T.; Zhang, Y. *Appl. Surf. Sci.* **1999**, *138*−*139*, 165.
(8) de Wilde, W.; de Mey, G. *Vacuum* **1974**, *24*, 307.
(9) Nason, T. C.; Moore, J. A.; Lu, T. M. *Appl. Phys. Lett.* **1992**, *60*, 1866.
(10) Usui, H.; Koshikawa, H.; Tanaka, K. *J. Vac. Sci. Technol., A* **1995**, *13*, 2318.
(11) Golub, M. A.; Wydeven, T.; Johnson, A. L. *Langmuir* **1998**, *14*, 2217 and references therein.
(12) Castner, D. G.; Lewis, K. B., Jr.; Fischer, D. A.; Ratner, B. D.; Gland, J. L. *Langmuir* **1993**, *9*, 537.
(13) Butoi, C. I.; Mackie, N. M.; Barnd, J. L.; Fisher, E. R.; Gamble, L. J.; Castner, D. G. *Chem. Mater.* **1999**, *11*, 862.
(14) Limb, S. J.; Labelle, C. B.; Gleason, K. K.; Edell, D. J.; Gleason, E. F. *Appl. Phys. Lett.* **1996**, *68*, 2810.
(15) Limb, S. J.; Lau, K. K. S.; Edell, D. J.; Gleason, E. F.; Gleason, K. K. *Plasmas Polym.* **1999**, *4*, 21.
(16) Lau, K. K. S.; Gleason, K. K. *J. Fluorine Chem.* **2000**, *104*, 119.
(17) Sargeant, P. B. *J. Org. Chem.* **1970**, *35*, 678.
(18) Mahler, W.; Resnick, P. R. *J. Fluorine Chem.* **1973**, *3*, 451.
(19) Kennedy, R. C.; Levy, J. B. *J. Fluorine Chem.* **1976**, *7*, 101.
(20) Lau, K. K. S.; Caulfield, J. A.; Gleason, K. K. *Chem. Mater.* **2000**, *12*, 3032.
(21) Lau, K. K. S.; Caulfield, J. A.; Gleason, K. K. *J. Vac. Sci. Technol., A* **2000**, *18*, 2404.
(22) Kerbow, D. L. Polytetrafluoroethylene (Overview). In *Polymeric Materials Encyclopedia*; Salamone, J. C., Ed.; CRC Press: Boca Raton, FL, 1996; Vol. 9, p 6884.
(23) Cruden, B.; Chu, K.; Gleason, K.; Sawin, H. *J. Electrochem. Soc.* **1999**, *146*, 4590.
(24) Cruden, B.; Chu, K.; Gleason, K.; Sawin, H. *J. Electrochem. Soc.* **1999**, *146*, 4597.
(25) Liang, C. Y.; Krimm, S. *J. Chem. Phys.* **1956**, *25*, 563.
(26) Moynihan, R. E. *J. Am. Chem. Soc.* **1959**, *81*, 1045.
(27) Roeges, N. P. G. *A Guide to the Complete Interpretation of Infrared Spectra of Organic Structures*; Wiley: New York, 1994.
(28) Fisher, W. K.; Corelli, J. C. *J. Polym. Sci., Part A: Polym. Chem.* **1981**, *19*, 2465.
(29) Kobayashi, M.; Sakashita, M.; Adachi, T.; Kobayashi, M. *Macromolecules* **1995**, *28*, 316.
(30) Savage, C. R.; Timmons, R. B.; Lin, J. W. *Chem. Mater.* **1991**, *3*, 575.
(31) Lau, K. K. S.; Gleason, K. K. *J. Phys. Chem. B* **1997**, *101*, 6839.
(32) Lau, K. K. S.; Gleason, K. K. *J. Phys. Chem. B* **1998**, *102*, 5977.
(33) Golden, J. H. *J. Polym. Sci.* **1960**, *45*, 534.
(34) Bro, M. I.; Lovejoy, E. R.; McKay, G. R. *J. Appl. Polym. Sci.* **1963**, *7*, 2121.
(35) Siegel, S.; Hedgpath, H. *J. Chem. Phys.* **1967**, *46*, 3904.
(36) Lerner, N. R. *J. Chem. Phys.* **1969**, *50*, 2902.
(37) Oshima, A.; Seguchi, T.; Tabata, Y. *Radiat. Phys. Chem.* **1997**, *50*, 601.
(38) Hedvig, P. *J. Polym. Sci., Part A: Polym. Chem.* **1969**, *7*, 1145.
(39) Iwasaki, M. *Fluorine Chem. Rev.* **1971**, *5*, 1.
(40) Fischer, D.; Lappan, U.; Hopfe, I.; Eichhorn, K. J.; Lunkwitz, K. *Polymer* **1998**, *39*, 573.
(41) Lunkwitz, K.; Brink, H.-J.; Handte, D.; Ferse, A. *Radiat. Phys. Chem.* **1989**, *33*, 523.
(42) Baker, B. B. J.; Kasprzak, D. J. *Polym. Degrad. Stab.* **1993**, *42*, 181.
(43) Lappan, U.; Häussler, L.; Pompe, G.; Lunkwitz, K. *J. Appl. Polym. Sci.* **1997**, *66*, 2287.
(44) Ferry, L.; Vigier, G.; Vassoille, R.; Bessede, J. L. *Acta Polym.* **1995**, *46*, 300.
(45) Lauritzen, J. I.; Hoffmann, J. D. *J. Appl. Phys.* **1973**, *44*, 4340.